

Challenges in simulating beam dynamics of dielectric laser acceleration

Uwe Niedermayer^{*,†}

*Technische Universität Darmstadt,
Institute for Accelerator Science and Electromagnetic Fields (TEMF),
Schlossgartenstrasse 8, D-64289 Darmstadt, Germany
niedermayer@temf.tu-darmstadt.de*

A. Adelman, S. Bettoni, M. Calvi, M. Dehler, E. Ferrari, F. Frei, D. Hauenstein,
B. Hermann, N. Hiller, R. Ischebeck, C. Lombosi, E. Prat, S. Reiche and L. Rivkin
Paul Scherrer Institut, CH-5232 Villigen, Switzerland

R. Aßmann, U. Dorda, I. Hartl, W. Kuroopka, F. Lemery, B. Marchetti,
F. Mayet, H. Xuan and J. Zhu
Deutsches Elektronen-Synchrotron, D-22607 Hamburg, Germany

D. S. Black, P. N. Broaddus, R. L. Byer, A. Ceballos, H. Deng, S. Fan, J. Harris,
T. Hirano, T. W. Hughes, Y. Jiang, T. Langenstein, K. Leedle, Y. Miao, A. Ody,
A. Pigott, N. Sapra, O. Solgaard, L. Su, S. Tan, J. Vuckovic, K. Yang and Z. Zhao
Stanford University, Stanford, CA 94305, USA

O. Boine-Frankenheim, T. Egenolf and E. Skär
Technische Universität Darmstadt, D-64289 Darmstadt, Germany

D. Cesar, P. Musumeci, B. Naranjo, J. Rosenzweig and X. Shen
University of California, Los Angeles, CA 90095, USA

B. Cowan
Tech-X Corporation, Boulder, CO 80303, USA

R. J. England and Z. Huang
SLAC National Accelerator Laboratory, Menlo Park, CA 94025, USA

H. Cankaya, M. Fakhari, A. Fallahi and F. X. Kärtner
*Center for Free-Electron Laser Science,
DESY and University of Hamburg, D-22607 Hamburg, Germany*

*Corresponding author.

†Visting postdoctoral scholar at Ginzton Lab, Stanford University (2018).

T. Feurer

Universität Bern, Switzerland

P. Hommelhoff, J. Illmer, A. Li, A. Mittelbach, J. McNeur, N. Schönenberger,
R. Shiloh, A. Tafel and P. Yousefi

Friedrich-Alexander Universität Erlangen-Nürnberg, 91058 Erlangen, Germany

M. Kozak

Charles University, 12116 Prague 2, Czech Republic

M. Qi and Y. J. Lee

Purdue University, West Lafayette, IN 47907, USA

Y.-C. Huang

Nat. Tsing Hua University, Taiwan

E. Simakov

Los Alamos National Laboratory, USA

Received 28 February 2019

Revised 15 June 2019

Accepted 17 June 2019

Published 26 November 2019

Dielectric Laser Acceleration (DLA) achieves the highest gradients among structure-based electron accelerators. The use of dielectrics increases the breakdown field limit, and thus the achievable gradient, by a factor of at least 10 in comparison to metals. Experimental demonstrations of DLA in 2013 led to the Accelerator on a Chip International Program (ACHIP), funded by the Gordon and Betty Moore Foundation. In ACHIP, our main goal is to build an accelerator on a silicon chip, which can accelerate electrons from below 100 keV to above 1 MeV with a gradient of at least 100 MeV/m. For stable acceleration on the chip, magnet-only focusing techniques are insufficient to compensate the strong acceleration defocusing. Thus, spatial harmonic and Alternating Phase Focusing (APF) laser-based focusing techniques have been developed. We have also developed the simplified symplectic tracking code DLAttrack6D, which makes use of the periodicity and applies only one kick per DLA cell, which is calculated by the Fourier coefficient of the synchronous spatial harmonic. Due to coupling, the Fourier coefficients of neighboring cells are not entirely independent and a field flatness optimization (similarly as in multi-cell cavities) needs to be performed. The simulation of the entire accelerator on a chip by a Particle In Cell (PIC) code is possible, but impractical for optimization purposes. Finally, we have also outlined the treatment of wake field effects in attosecond bunches in the grating within DLAttrack6D, where the wake function is computed by an external solver.

Keywords: Dielectric; laser; accelerator; chip; ACHIP.

1. Introduction

The Accelerator on a Chip International Program (ACHIP),¹ funded by the Gordon and Betty Moore Foundation in the period between 2015 and 2020, aims to explore

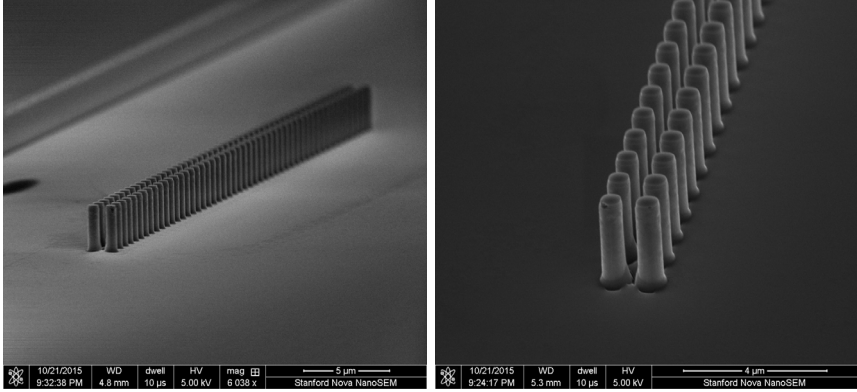


Fig. 1. Scanning Electron Microscope (SEM) pictures of a dual pillar acceleration structure.

Dielectric Laser Acceleration (DLA). This nascent acceleration scheme provides the highest gradients among structure-based (nonplasma, nonvacuum, etc.) electron accelerators and thus allows reduction of the size of high energy electron accelerators significantly. The principle of DLA relies on the inverse Smith–Purcell (or the inverse Cherenkov effect) and was first proposed in 1962.^{2,3} In 2013, the acceleration of relativistic electrons was first demonstrated at SLAC with a gradient of more than 250 MeV/m in an SiO₂ double grating structure driven by a 800 nm Ti:Sapphire laser.⁵ In the same setup, the gradient was later increased to 690 MeV/m.⁶ Also, in 2013, strongly sub-relativistic electrons (27.7 keV) were accelerated by the group at FAU Erlangen with a gradient of 25 MeV/m using a single grating structure at the third spatial harmonic.⁷ The group at Stanford University used a silicon dual pillar structure to accelerate 96 keV electrons with a gradient of more than 200 MeV/m⁸ and a similar experiment at 30 keV with few-cycle laser pulses was done at FAU Erlangen.⁹ An example of such a dual pillar structure is shown in Fig. 1. These schemes all utilize laterally incident lasers with polarization in the electron beam direction, thus the accelerating near field is a standing wave. It is also possible to use longitudinally coupled (traveling wave) structures, see Refs. 10 and 11 for details and a general overview. Another option using a quite simple structure is to excite surface waves by total internal reflection in flat dielectrics.⁴

The goal of ACHIP is to build an accelerator as sketched in Fig. 2, which can accelerate electrons from electrostatic sources (< 100 keV) to above 1 MeV. A second goal is to make use of the accelerator by exploring the options of DLA-based deflection (see e.g. Ref. 12), which can potentially lead to laser-driven undulators.^{13–15}

Different materials have been investigated for DLA.¹⁶ In order to achieve the highest gradient, the material-specific damage threshold fluence

$$F_{\text{dam}} > F = \frac{P\Delta t}{A}, \quad (1)$$

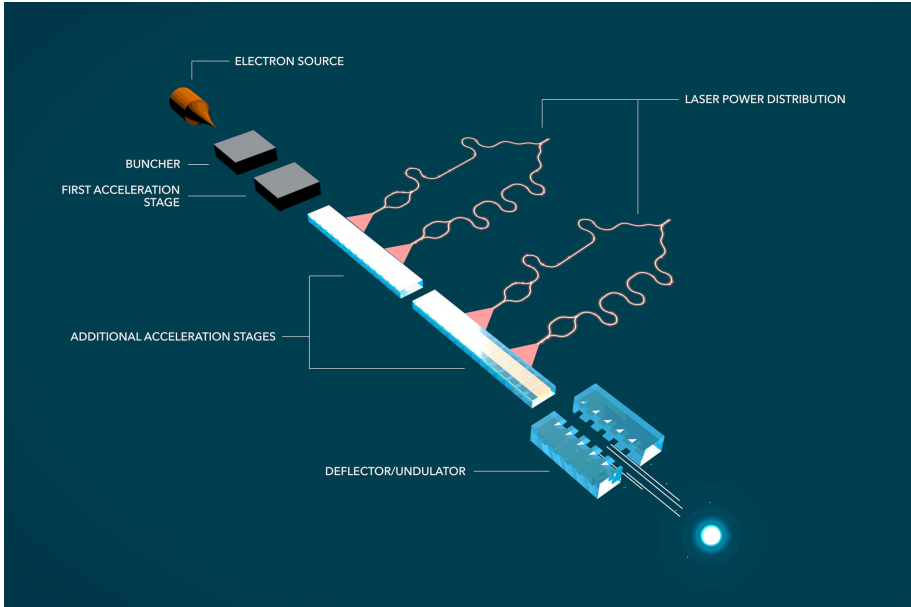


Fig. 2. Sketch of the goals of the ACHIP collaboration.

where P/A is the laser intensity and Δt is the pulse length, is approached, but must not be exceeded. Note that the dependence on the laser wavelength and pulse length can be strongly nonlinear, see e.g. Ref. 17 for an in-depth discussion and more empirical data. Moreover, if the laser travels a longer distance through the material, the nonlinear phase shift also needs to be considered.¹⁸ In general, a shorter pulse allows for a higher gradient at the same fluence. Moreover, a high band gap material as e.g. SiO_2 will have a higher damage threshold and a low band gap material such as Silicon has a lower damage threshold but a higher refractive index.

For the sub-relativistic experiments in the ACHIP collaboration, we mostly use $\lambda_0 = 2 \mu\text{m}$ femtosecond laser pulses, generated by Optical Parametric Amplifiers (OPA) or by novel Tm or Ho-Tm fiber laser amplifiers currently under development. The electron source needs to provide ultra-low emittance, particularly at low energy. For a lossless sub-100-keV injection into a DLA operating at $2 \mu\text{m}$, geometric emittances smaller than 0.1 nm are required.¹⁹ Different emitters are available to produce these low emittances, e.g. Ref. 20, or see Ref. 21 for an overview. At these emittances, the achievable charge is quite small at the moment. We hope to achieve higher average charge in the future by increasing both the repetition rate and the single microbunch charge.

2. Different Means of Laser Coupling

All the DLA experiments published so far have used free space laser coupling. At longer interaction length, it is necessary to provide symmetric fields, such that there

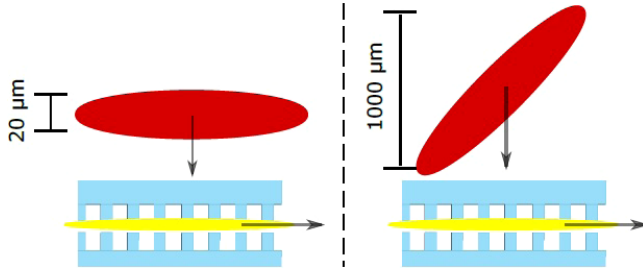


Fig. 3. Flat versus tilted laser pulse. At roughly the same pulse length for each grating cell, the interaction length is significantly increased. Picture adapted from Ref. 25.

is no coherent deflection force. There are different means to obtain symmetric fields in the acceleration channel, the simplest is to illuminate the structure symmetrically from both sides with equal phase and polarization. If this is impractical from the optics point of view, the fields of a single side drive laser can also be symmetrized by using a Bragg mirror on the chip.^{22,23}

The laser fluence on each DLA cell can be reduced by shortening the pulse and tilting the pulse front,^{25,26} such that it remains synchronous with a few electron bunches over a distance (or duration) much longer than a single DLA cell is illuminated, see Fig. 3. Practically, the pulse front tilt can be achieved, for example, by a prism or by a reflection grating with unequal incidence and reflection angles.^{24–26}

Another option to increase the interaction length in the accelerator structure is an on-chip waveguide system,²⁷ see Fig. 4. This supplies different parts of the accelerator structure with the appropriate phase and group delay. Moreover, a different higher damage threshold and lower refractive index material can be used to convey higher laser fluence in the waveguides, which can be split into many waveguides

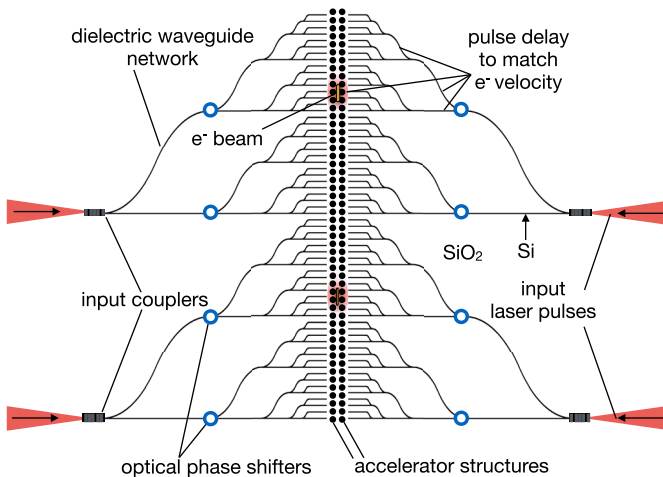


Fig. 4. On-chip waveguide laser power delivery system. Picture adapted from Ref. 27.

before coupling to the high refractive index accelerator structure. Using this technique, it is possible to produce a similar illumination pattern as would be obtained by pulse front tilt in free space.

3. Field Computation for a Single DLA Cell

The laser field computation of a single DLA cell using periodic boundary conditions is not a challenge, since its electrical length L/λ is on the order of one. It can be simulated by various techniques such as Finite Difference/Finite Integration Time Domain (FD/FI TD) codes,^{28,29} Finite Difference Frequency Domain (FDFD) codes,³⁰ or Finite Element Frequency Domain (FEFD) codes.^{29,31} These can be combined with various optimization techniques, in order to find structures with highest gradient, lowest field inside the material, or highest bandwidth. Of course, these optimization goals compete, such that an optimum can only be found in the sense of a Pareto-front. Simple DLA structures can also be designed from a physical point of view, such that maximum electric field modulation at the synchronous harmonic is achieved, which results in Bragg cavity structures.^{31,32} A more mathematical approach is rather to use adjoint methods to perform large-scale, gradient-based optimization of the full permittivity distribution.³⁴ However, these methods tend to generate nonintuitive device geometries and sometimes require additional constraints to create fabricable structures. Moreover, adjoint methods have also been used for other parts of the integrated DLA, such as grating couplers.³⁵

4. Beam Dynamics Simulations in DLATRACK6D

We will summarize and slightly add to DLATRACK6D, the one kick per cell tracking approach originally conceived in Ref. 32. The kicks are sufficiently described by one complex coefficient per DLA cell, where the longitudinal and transverse dependencies are derived analytically. Although the derivation holds true only for strict periodicity, small deviations can be accepted within reasonable error. Also, fringe fields are not included, even in practice they should be reduced as much as possible. The effect of fringe fields is however strongly dependent on the quality factor of the structure, usually determined by the available bandwidth.

Starting from the longitudinal energy gain, the kicks in all directions are computed and then used for symplectic tracking. The energy gain of an electron with charge $q = -e$ can be written as function of the time domain electric field E_z , its Frequency Domain (FD) phasor \underline{E}_z , or by means of spatial Fourier series in periodic DLA structures

$$\Delta W(x, y, s) = q \int_{-\lambda_{gz}/2}^{\lambda_{gz}/2} E_z(x, y, z; t = (z + s)/v) dz \quad (2)$$

$$= q \lambda_{gz} \operatorname{Re} \left\{ e^{2\pi i \frac{s}{\beta \lambda_0}} \underline{e}_m(x, y) \right\}. \quad (3)$$

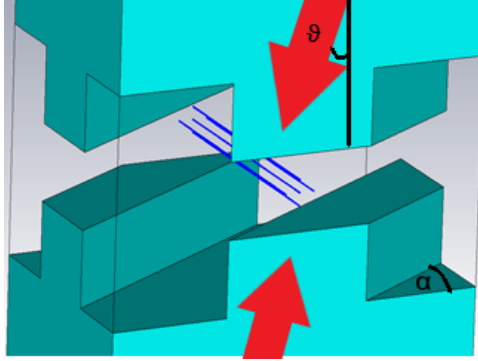


Fig. 5. Unit cell of a tilted grating (tilt angle α , where $\alpha = 0$ is a straight, infinitely wide grating). The blue lines indicate possible electron trajectories. The laser is incident from top and bottom, with polarization in electron beam direction and possible tilt angle ϑ in the plane perpendicular to the electron beam.

Here, the spatial Fourier coefficient is computed as

$$\underline{e}_m(x, y) = \frac{1}{\lambda_{gz}} \int_{-\lambda_{gz}/2}^{\lambda_{gz}/2} \underline{E}_z(x, y, z) e^{im \frac{2\pi}{\lambda_{gz}} z} dz. \quad (4)$$

The above relation holds only if the Wideroe condition $\lambda_{gz} = m\beta\lambda_0$ is fulfilled, where λ_{gz} is the grating period and β is the velocity in units of c . In the following we will restrict the arbitrary integer spatial harmonic m to $m = 1$, which usually has the strongest amplitude \underline{e}_1 . For the application of higher harmonics see e.g. Ref. 33.

The transverse kicks can be obtained by exploiting the known transverse dependency of $\underline{e}_1(x, y)$ on the transverse coordinates. From the Panofsky–Wenzel theorem,³⁶ conveniently written as

$$\nabla' \times \Delta \mathbf{p}(x, y, s) = 0, \quad (5)$$

where the relative gradient is $\nabla' = (\partial_x, \partial_y, -\partial_s)$, we obtain under the synchronicity condition³²

$$\Delta \mathbf{p}_\perp(x, y, s) = -\frac{\lambda_{gz}^2}{2\pi} q \frac{1}{\beta c} \text{Im}\{e^{2\pi i \frac{s}{\beta\lambda_0}} \nabla_\perp \underline{e}_1(x, y)\}. \quad (6)$$

For a symmetric laser illumination, the transverse dependencies can be written as

$$\underline{e}_1(x, y) = \underline{e}_1(0, 0) \cosh(ik_y y) e^{ik_x x}, \quad (7)$$

where k_x includes the option of a tilt of the grating or the laser incidence, $k_z = 2\pi/(\beta\lambda_0)$, and $k_y = \pm\sqrt{(2\pi/\lambda_0)^2 - k_z^2 - k_x^2}$. For a grating tilt angle α (see Fig. 5) we obtain³² $k_x = k_z \tan(\alpha)$ and for a laser tilt angle θ (keeping the polarization parallel to the electron beam) we obtain $k_x = k_z \sin(\theta)$. After some manipulations, we finally obtain the kicks³²

$$\Delta x' = -\frac{q\lambda_0}{p_{z0}c} \tan(\alpha) \cosh(ik_y y) \text{Re}\{\underline{e}_1 e^{i\varphi + ik_x x}\}, \quad (8a)$$

$$\Delta y' = \frac{-ik_y \lambda_0^2 q \beta}{2\pi p_{z0} c} \sinh(ik_y y) \text{Im}\{\underline{e}_1 e^{i\varphi + ik_x x}\}, \quad (8b)$$

$$\Delta \delta = \frac{q \lambda_{gz}}{\gamma m_e c^2} \text{Re}\{\underline{e}_1 (\cosh(ik_y y) e^{i\varphi + ik_x x} - e^{i\varphi_s})\}. \quad (8c)$$

In case of an anti-symmetric illumination, i.e. a π phase shift between the two laser beams, the transverse dependence is

$$\underline{e}_1(x, y) = \underline{e}_1(0, 0) \sinh(ik_y y) e^{ik_x x}, \quad (9)$$

and the kicks are accordingly

$$\Delta x' = -\frac{q \lambda_0}{p_{z0} c} \tan(\alpha) \sinh(ik_y y) \text{Re}\{\underline{e}_1 e^{i\varphi + ik_x x}\}, \quad (10a)$$

$$\Delta y' = \frac{-ik_y \lambda_0^2 q \beta}{2\pi p_{z0} c} \cosh(ik_y y) \text{Im}\{\underline{e}_1 e^{i\varphi + ik_x x}\}, \quad (10b)$$

$$\Delta \delta = \frac{q \lambda_{gz}}{\gamma m_e c^2} \text{Re}\{\underline{e}_1 \sinh(ik_y y) e^{i\varphi + ik_x x}\}. \quad (10c)$$

Note that in the sinh-mode, the energy gain of the synchronous particle is always zero, since the longitudinal electric field vanishes in the center of the channel. The sinh-mode can be used as a diagnostic, in order to convert a temporal profile into an angle distribution profile,³⁷ which is usually referred to as beam streaking.

The symplectic one-kick-per-cell tracking is independent of the realization of the kick functions and reads

$$\begin{pmatrix} x \\ x' \\ y \\ y' \\ \varphi \\ \delta \end{pmatrix}^{(n+1)} = \begin{pmatrix} x \\ Ax' + \Delta x' \\ y \\ Ay' + \Delta y' \\ \varphi \\ \delta + \Delta \delta(\varphi_s) \end{pmatrix}^{(n)} + \begin{pmatrix} \lambda_{gz} x' \\ 0 \\ \lambda_{gz} y' \\ 0 \\ -\frac{2\pi}{\beta^2 \gamma^2} \delta \\ 0 \end{pmatrix}^{(n+1)}, \quad (11)$$

with the tracking variables in paraxial approximation

$$\begin{aligned} x' &= \frac{p_x}{p_{z0}}, & \Delta x' &= \frac{\Delta p_x(x, y, \varphi)}{p_{z0}}, \\ y' &= \frac{p_y}{p_{z0}}, & \Delta y' &= \frac{\Delta p_y(x, y, \varphi)}{p_{z0}}, \\ \varphi &= 2\pi \frac{s}{\lambda_{gz}}, & \delta &= \frac{W - W_0}{W_0}, \\ \Delta \delta &= \frac{\Delta W(x, y, \varphi) - \Delta W(0, 0, \varphi_s)}{W_0}, \end{aligned} \quad (12)$$

where $W_0 = \gamma m_e c^2$ and $p_{z0} = \beta \gamma m_e c$. The adiabatic damping of the transverse emittance is described by

$$A^{(n)} = \frac{(\beta\gamma)^{(n+1)}}{(\beta\gamma)^{(n)}} = 1 + \left[\frac{\lambda_0 q \operatorname{Re}\{e^{i\varphi_s} \underline{e}_1\}}{\beta\gamma m_e c^2} \right]^{(n)}. \quad (13)$$

While keeping the synchronicity condition by appropriately chirping the structure, the acceleration ramp can be written as

$$W(N) = W(0) + q \sum_{n=1}^N \lambda_g^{(n)} \operatorname{Re}\{e_1^{(n)} e^{i\varphi_s^{(n)}}\}. \quad (14)$$

We note that chirping the structure length while maintaining constant phase $\arg(\underline{e}_1)$ is possible by correcting the phase drift with another parameter in the structure design.²²

DLAtrack6D is written in Matlab,³⁸ it is based on a phase space structure that allows for vectorized updates in each DLA cell. The code, together with a brief manual, is available upon request.

5. Electron Beam Focusing

Optical near field accelerators cannot rely on magnetic focusing only, since the small scale of the near field requires sub-micron beam sizes which in turn would require magnetic field strengths unachievable by conventional quadrupole magnets.³⁹ Thus, a laser-based focusing scheme is required to make DLA scalable.

Two different options have been proposed for focusing with the phase-dependent transverse laser fields. In 2012, the group at UCLA has proposed spatial harmonic focusing.⁴⁰ Stability of the electron beam could be predicted by means of retracting ponderomotive forces due to nonsynchronous harmonics, while the synchronous harmonic serves for acceleration. However, the beam envelope at given emittance could not be determined more accurately than in the smooth approximation. Moreover, the focusing harmonic needs to be quite strong (much stronger than the accelerating harmonic), which puts a constraint on the choice of materials and pulse length due to the damage threshold fluence. In particular, this scheme has been implemented with SiO₂ structures at relativistic energies.⁴¹

Recently, Niedermayer *et al.* proposed Alternating Phase Focusing (APF) for DLA.¹⁹ Here, we work only with a single spatial harmonic, i.e. \underline{e}_1 , but its phase can be changed by means of fractional period drift elements. The hereby generated longitudinal/transversal alternating focusing gradients can be integrated in the Courant–Snyder sense. Thus, a scalable scheme is obtained, where about half (dependent on the synchronous phase) of the synchronous harmonic is translated to acceleration gradient. The required pre-bunching on the optical scale can be obtained with the same scheme, see Ref. 19. Due to the exact integration of the lattice (and thus a precise determination of the beam envelope) and the efficient translation of incident field to acceleration gradient, this scheme is particularly suited

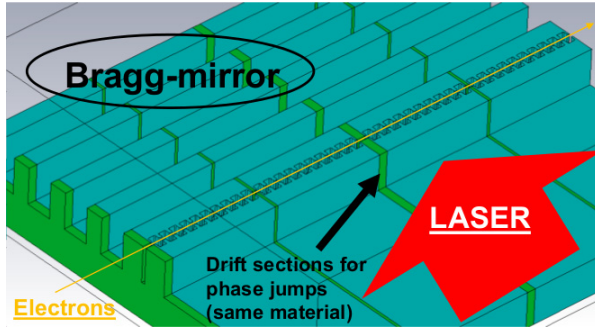


Fig. 6. Outline of an APF DLA structure, picture adapted from Ref. 32.

for sub-relativistic DLAs working with high refractive index Silicon structures that have a rather low damage threshold. An outline of such a structure is depicted in Fig. 6. Such APF-structures are capable of confining the electron beam in longitudinal and horizontal direction. The confinement in the vertical direction, where the laser fields are ideally invariant, can be achieved by enclosing the entire chip by a vertically focusing quadrupole magnet, which can be realized with Neodymium permanent magnets.

6. Full Scale Simulation Techniques

For full scale tracking and Particle In Cell (PIC) simulations, we mostly use the codes CST Studio Suite²⁹ and VSim.²⁸ A full scale PIC simulation is however numerically quite heavy, thus we prefer to do this only for finished designs and rely on DLATRACK6D for design studies. In CST, we have the convenient option to calculate the fields either in TD or FD and store them as frequency domain phasors, i.e. one complex number per mesh edge. Note that storing in FD does not necessary mean computation in FD; in fact, FD simulations become intractable as the simulation size becomes large, so instead, TD computation can be performed along with an on-the-fly Fourier Transform.

We use VSim in cases where large scale computing is required. Moreover, including a pulse front tilted laser beam is rather involved in CST at the moment, thus we did this in VSim. The capability of VSim for electron energy loss in materials, to model experiments where part of the electron beam clips the structure, was also added and showed good agreement with experiments.⁶ In the near future, we plan to conduct high performance PIC simulations to assess the effects of fringe fields and imperfect field flatness, wake fields, and radiation emission using NERSC cluster time awarded to the ACHIP collaboration partner TechX.

7. Recently Completed and Ongoing Experiments

Simulations are conducted for the design and the evaluation of different recent DLA experiments. Recently completed were experiments for acceleration with displaced

dual pillar structures and Bragg reflectors.⁴² Moreover, the first acceleration results with waveguide driven inverse-designed DLA structures were obtained recently.⁴³

The first focusing experiment uses the intrinsic phase-dependent focusing properties of a DLA structure.⁴⁴ In this experiment, the electrons are injected at random phase, which means that they are either focused or defocused, i.e. a cross-shape is formed in transverse phase space (see also Ref. 22). An aperture lets only the focused electrons pass, the defocused ones are lost. This transmission is however still higher than in the absence of the laser, i.e. when there is no focusing at all. This experiment can also be run in deflection (sinh) mode, i.e. the electrons are deflected to the left or right, dependent on their phase. Strong deflection will reduce the transmission through the aperture accordingly, which is readily measurable.

Another ongoing focusing experiment is APF with a Bragg mirror, as outlined in Fig. 7. As discussed in detail in Ref. 19, this APF focusing channel transports particles at all phases. A pre-bunching is not required for transport only, however it would be required for acceleration. In the bottom of the figure, the longitudinal electric field is plotted. Different options for filling the half cell spaces for phase jumps have been simulated. In the end, it turned out that the spacers are only helpful in the beginning and the end of the structure and within it is sufficient to leave half a cell empty. Moreover, another crucial optimization is to tune the Bragg mirror distance such that the fields in the channel become symmetric. After the optimized fields have been determined, electron tracking can be done both in DLAttrack6D and full PIC codes. Figure 8 shows how the fraction of electrons transported through the structure is dependent on the laser field strength (DLAttrack6D). This structure has recently been fabricated (see Fig. 9) and is ready for testing at FAU Erlangen.

The minimal beta-function is obtained at roughly 200 MV/m, where maximum transmission occurs. Beyond that point, the beam is first over-focused, and eventually leaves the area of stability. The reason for the losses at the matched e_1 is the geometric emittance of 0.3 nm (Gaussian distribution initially), which is larger than

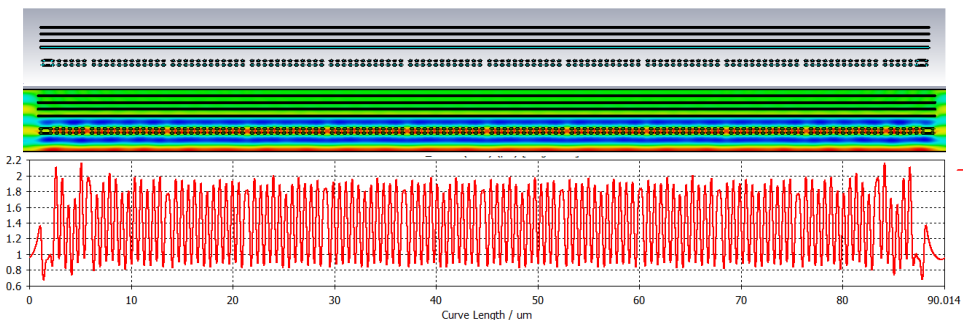


Fig. 7. (Color online) APF single laser beam transport structure (top), normalized (to 1 V/m incident laser field) longitudinal electric field phasor magnitude with laser from bottom (center) and on axis normalized field flatness plot (bottom), obtained by CST MWS in TD. The linear color scale reaches from 0 (blue) to 2 (red).

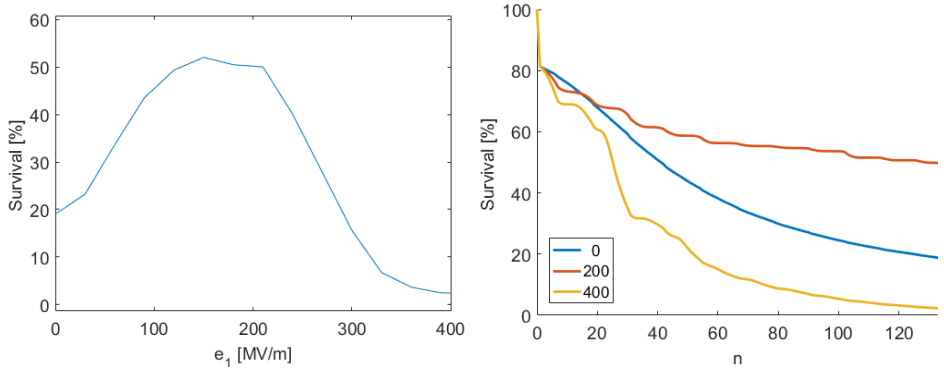


Fig. 8. Transmission rate as function of laser field strength (left) and electron loss as function of DLA cell index for $e_1 = (0, 200, 400)$ MV/m laser field strength (right).

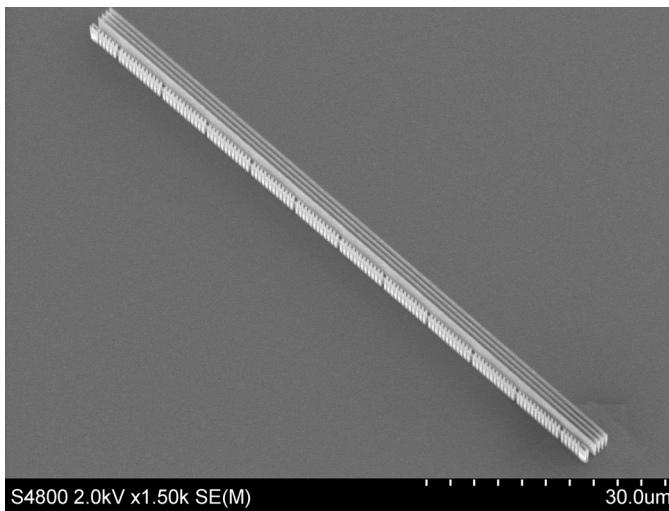


Fig. 9. SEM picture of the structure design as in Fig. 7.

the acceptance of the structure. Once saturated at about 50%, the electrons can be transported over an arbitrary distance, which is limited only by the defocusing in the direction of the pillar height. Roughly the same results are obtained by tracking in the CST PIC solver.

In succession to Refs. 37, 45 and 46, we plan a two stage buncher-accelerator or buncher-streaker experiment, see Fig. 10. Here, we use dual drive from two stages, with independent phase control and independent amplitude control of lasers 1 and 2. The first DLA stage is normally run in cosh-mode and serves as a buncher. The second stage can be either run in cosh-mode for acceleration, or in sinh-mode for streaking. Replacing the first (buncher) structure by an APF-type buncher, see Ref. 19, will allow us to obtain short bunches with low energy spread. This gives

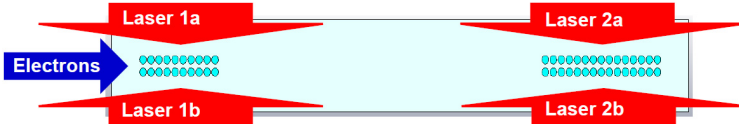


Fig. 10. Combined buncher and accelerator/streaker DLA.

the opportunity to observe both coherent streaking and coherent acceleration at the same setup on a spectrometer screen.

Additionally to the low energy experiment, there are also high-energy experiments planned. Most prominently, we will use the 3.2 GeV beam at SwissFEL at PSI to inject into a DLA. Due to the extremely small geometric emittance at such high energy, this injection will be almost lossless. Additionally, at such energy, the deflection and acceleration defocusing is rather small. Therefore, we are restricted only by the conventional electron optics (Rayleigh length) and the available laser pulse energy, which can be cast in a tilted pulse. Details of the outlined experiments can be found in Refs. 47 and 48.

Moreover, relativistic energy experiments are also outlined at the SINBAD facility at DESY, where an inverse FEL undulator together with a chicane will be employed for optical-scale bunching of the beam before it is injected into the DLA. Driving the DLA with the same laser as is used for seeding the inverse FEL allows for the precise phase control required for coherent acceleration.⁴⁹

The group at UCLA aims for a 2-cm long DLA experiment at about 5 MeV injection energy at the Pegasus facility.⁵⁰ Challenges are that focusing of the beam is still required and also a slight chirp needs to be imprinted to account for the slightly sub-relativistic velocity. Creating both the focusing harmonics and the chirp is planned to be achieved by a strictly periodic SiO₂ grating fed by a tilted laser pulse that is modulated by a Spatial Light Modulator, see e.g. Ref. 51.

8. Current Status and Outlook

We are now able to perform start-to-end simplified simulations of larger DLA chips with DLATRACK6D. For full scale 3D PIC or tracking simulations, a cluster computer is required. The experiments performed at the moment can still be simulated well in 2D by available PIC codes. However, it is expected that the structure lengths will soon significantly increase.

One option for efficient large-scale PIC for DLA would be a moving window code, which discretizes only the co-moving environment of a few electron micro-bunches. The rest of the structure contains neither electrons nor laser energy, since we strongly restrict the interaction region by applying the pulse front tilt or other means of selective synchronized illumination.

The charge we accelerate in current DLA experiments is mostly rather low. However, at particular high energy experiments as e.g. at PSI, the entire beam is

put through the small aperture of the DLA. We expect to see wake field effects here for the first time. Simulations of wake field effects are already in place.⁵² We outline to integrate linear and nonlinear wake kicks from precomputed wake functions into DLATRACK6D as well. With this we will be able to properly predict the strength of beam loading effects and longitudinal and transverse beam instabilities in longer DLA structures.

Acknowledgments

ACHIP is funded by the Gordon and Betty Moore Foundation (Grant No. GBMF4744 to Stanford). U.N. acknowledges also the funding by the German Federal Ministry of Education and Research (Grant No. FKZ:05K16RDB). B.C. (TechX) acknowledges usage of NERSC, a U.S. Department of Energy Office of Science User Facility operated under Contract No. DE-AC02-05CH11231.

References

1. ACHIP website: <https://achip.stanford.edu>.
2. K. Shimoda, *Appl. Opt.* **1**, 33 (1962).
3. A. Lohmann, IBM Technical Note, 169 (1962).
4. M. Kozak *et al.*, *Opt. Exp.* **25**, 19195 (2017).
5. E. A. Peralta *et al.*, *Nature* **503**, 91 (2013), doi:10.1038/nature12664.
6. K. P. Wootton *et al.*, *Opt. Lett.* **41**, 2696 (2016).
7. J. Breuer and P. Hommelhoff, *Phys. Rev. Lett.* **111**, 134803 (2013).
8. K. J. Leedle, A. Ceballos, H. Deng, O. Solgaard, R. Fabian Pease, R. L. Byer and J. S. Harris, *Opt. Lett.* **40**, 4344 (2015).
9. M. Kozak *et al.*, *NIM A* **865**, 84 (2017).
10. R. J. England *et al.*, *Rev. Mod. Phys.* **86**, 1337 (2014).
11. K. P. Wootton, J. Mcneur and K. J. Leedle, *Rev. Accel. Sci. Tech.* **09**, 105 (2016).
12. J. McNeur *et al.*, *Optica* **5**, 687 (2018), doi:10.1364/OPTICA.5.000687.
13. T. Plettner and R. L. Byer, *Phys. Rev. ST Accel. Beam* **11**, 030704 (2008).
14. T. Plettner and R. L. Byer, *Nucl. Instrum. Methods Phys. Res. A* **593**, 63 (2008).
15. T. Plettner, R. Byer, C. McGuinness and P. Hommelhoff, *Phys. Rev. ST Accel. Beams* **12**, 101302 (2009).
16. K. Soong, R. L. Byer, E. R. Colby, R. J. England and E. A. Peralta, *AIP Conf. Proc.* **1507**, 511 (2012).
17. P. Pronko *et al.*, *Phys. Rev. B* **58**, 2387 (1998).
18. D. Cesar *et al.*, *Nat. Comm. Phys.* **1**, 46 (2018).
19. U. Niedermayer, T. Egenolf, O. Boine-Frankenheim and P. Hommelhoff, *Phys. Rev. Lett.* **121**, 214801 (2018).
20. D. Ehberger, J. Hammer, M. Eisele, M. Krueger, J. Noe, A. Hogele and P. Hommelhoff, *Phys. Rev. Lett.* **114**, 227601 (2015).
21. A. Feist *et al.*, *Ultramicroscopy* **176**, 63 (2017).
22. U. Niedermayer, O. Boine-Frankenheim and T. Egenolf, *J. Phys. Conf. Ser.* **874**, 012041 (2017), doi:10.1088/1742-6596/874/1/012041.
23. P. Yousefi *et al.* *Nucl. Instrum. Methods A* **909**, 221 (2018).
24. Y. Wei *et al.*, *Appl. Opt.* **56**, 8201 (2017).
25. D. Cesar, J. Maxson, P. Musumeci, X. Shen, R. J. England and K. P. Wootton, SLAC-PUB-17180 (2017).

26. M. Kozak *et al.*, *J. Appl. Phys.* **124**, 023104 (2018), doi:10.1063/1.5032093.
27. T. W. Hughes *et al.*, *Phys. Rev. Appl.* **9**, 54017 (2018).
28. VSim, www.txcorp.com.
29. CST Studio Suite 2018, www.cst.com.
30. W. Shin and S. Fan, *Opt. Express* **21**, 22578 (2013).
31. T. Egenolf, O. Boine-Frankenheim and U. Niedermayer, *J. Phys.: Conf. Ser.* **874**, 012040 (2017), doi:10.1088/1742-6596/874/1/012040.
32. U. Niedermayer, T. Egenolf and O. Boine-Frankenheim, *Phys. Rev. AB* **20**, 111302 (2017).
33. J. McNeur, M. Kozak, D. Ehberger, N. Schöenberger, A. Tafel, A. Li and P. Hommelhoff, *J. Phys. B: At. Mol. Opt. Phys.* **49**, 034006 (2016).
34. T. Hughes *et al.*, *Opt. Express* **25**, 15414 (2017), doi:10.1364/OE.25.015414.
35. N. Sapra *et al.*, *IEEE JSTQE* **25** (2019).
36. W. K. H. Panofsky and W. A. Wenzel, *Rev. Sci. Instrum.* **27**, 967 (1956), doi:10.1063/1.1715427.
37. K. J. Leedle, D. S. Black, Y. Miao, K. E. Urbanek, A. Ceballos, H. Deng, J. S. Harris, O. Solgaard and R. L. Byer, *Opt. Lett.* **43**, 2181 (2018).
38. MathWorks, Matlab (2016).
39. A. Ody, P. Musumeci, J. Maxson, D. Cesar, R. J. England and K. P. Wootton, *NIM A* **865**, 75 (2017).
40. B. Naranjo, A. Valloni, S. Putterman and J. B. Rosenzweig, *Phys. Rev. Lett.* **109**, 164803 (2012).
41. D. Cesar, J. Maxson, X. Shen, K. P. Wootton, S. Tan, R. J. England and P. Musumeci, *Opt. Express* **26**, 29216 (2018) 1804.00634.
42. P. Yousefi, N. Schöenberger, J. McNeur, M. Kozak, U. Niedermayer and P. Hommelhoff, *Opt. Lett.* **44**, 1520 (2019).
43. N. Sapra *et al.*, 1905.12822.
44. D. Black, K. Leedle, Y. Miao, U. Niedermayer, R. L. Byer and O. Solgaard, *Phys. Rev. Lett.* **122**, 104801 (2019).
45. M. Kozak *et al.*, *Nat. Comm.* **8**, 14342 (2017).
46. M. Kozak, N. Schöenberger and P. Hommelhoff, *Phys. Rev. Lett.* **120**, 103203 (2018).
47. E. Prat *et al.*, *NIM A* **865**, 87 (2017).
48. E. Ferrari *et al.*, *NIM A* **907**, 244 (2018).
49. F. Mayet *et al.*, *NIM A* **909**, 213 (2018).
50. D. Cesar, P. Musumeci and R. J. England, *2018 IEEE Advanced Accelerator Concepts Workshop (AAC)*, doi:10.1109/AAC.2018.8659380.
51. ThorLabs EXULUS-HD1 Spatial Light Modulator, www.thorlabs.com.
52. T. Egenolf, U. Niedermayer and O. Boine-Frankenheim, *2018 IEEE Advanced Accelerator Concepts Workshop (AAC)*, doi:10.1109/AAC.2018.8659426.